FWM-based wavelength conversion of 40 Gbaud PSK signals in a silicon germanium waveguide

Mohamed A. Ettabib,[1] Kamal Hammani,[1] Francesca Parmigiani,[1] Liam Jones,[1] Alexandros Kapsalis,[2] Adonis Bogris,[2, 3] Dimitris Syvridis,[2] Mickael Brun,[4] Pierre Labeye,[4] Sergio Nicoletti,[4] and Periklis Petropoulos[1]

[1]Optoelectronics Research Centre, University of Southampton, Southampton, SO17 1BJ, UK
[2]National and Kapodistrian University of Athens, Panepistimiopolis, Ilissia, 15784, Athens, Greece
[3]Department of Informatics, Technological Educational Institute of Athens, Aghiou Spiridonos, 12210 Egaleo, Athens, Greece
[4]CEA, LETI, MINATEC Campus, F-38054 Grenoble, France
** mae206@orc.soton.ac.uk*

Abstract: We demonstrate four wave mixing (FWM) based wavelength conversion of 40 Gbaud differential phase shift keyed (DPSK) and quadrature phase shift keyed (QPSK) signals in a 2.5 cm long silicon germanium waveguide. For a 290 mW pump power, bit error ratio (BER) measurements show approximately a 2-dB power penalty in both cases of DPSK (measured at a BER of 10^{-9}) and QPSK (at a BER of 10^{-3}) signals that we examined.

OCIS codes: (130.3120) Integrated optics devices; (130.7405) Wavelength conversion devices; (190.4390) Nonlinear optics, integrated optics; (190.4380) Nonlinear optics, four-wave mixing; (230.7390) Waveguides, planar.

References and links

1. J. Hansryd, P. A. Andrekson, M. Westlund, Jie Li, and P.-O. Hedekvist, "Fiber-based optical parametric amplifiers and their applications," IEEE J. Sel. Top. Quantum Electron. **8**(3), 506–520 (2002).
2. C. Koos, L. Jacome, C. Poulton, J. Leuthold, and W. Freude, "Nonlinear silicon-on-insulator waveguides for all-optical signal processing," Opt. Express **15**(10), 5976–5990 (2007).
3. M. A. Foster, A. C. Turner, J. E. Sharping, B. S. Schmidt, M. Lipson, and A. L. Gaeta, "Broad-band optical parametric gain on a silicon photonic chip," Nature **441**(7096), 960–963 (2006).
4. L. Oxenlowe, H. Mulvad, H. Hu, H. Ji, M. Galili, M. Pu, K. Yvind, J. Hvam, P. Jeppesen, E. Palushani, and A. Clausen, "Ultrafast nonlinear signal processing in silicon waveguides," OFC, OTh3H.5 (2012).
5. Q. Lin, O. J. Painter, and G. P. Agrawal, "Nonlinear optical phenomena in silicon waveguides: Modeling and applications," Opt. Express **15**(25), 16604–16644 (2007).
6. H. Rong, A. Liu, R. Jones, O. Cohen, D. Hak, R. Nicolaescu, A. Fang, and M. Paniccia, "An all-silicon Raman laser," Nature **433**(7023), 292–294 (2005).
7. D. Liang and J. Bowers, "Recent progress in lasers on silicon," Nat. Photonics **4**(8), 511–517 (2010).
8. R. Claps, D. Dimitropoulos, V. Raghunathan, Y. Han, and B. Jalali, "Observation of stimulated Raman amplification in silicon waveguides," Opt. Express **11**(15), 1731–1739 (2003).
9. H. Fukuda, K. Yamada, T. Shoji, M. Takahashi, T. Tsuchizawa, T. Watanabe, J. Takahashi, and S. Itabashi, "Four-wave mixing in silicon wire waveguides," Opt. Express **13**(12), 4629–4637 (2005).
10. B. G. Lee, A. Biberman, A. C. Turner-Foster, M. A. Foster, M. Lipson, A. L. Gaeta, and K. Bergman, "Demonstration of broadband wavelength conversion at 40 Gb/s in silicon waveguides," IEEE Photon. Technol. Lett. **21**(3), 182–184 (2009).
11. B. Corcoran, C. Monat, C. Grillet, D. J. Moss, B. J. Eggleton, T. P. White, L. O'Faolain, and T. F. Krauss, "Green light emission in silicon through slow-light enhanced third-harmonic generation in photonic crystal waveguides," Nat. Photonics **3**(4), 206–210 (2009).
12. E. Dulkeith, Y. A. Vlasov, X. Chen, N. C. Panoiu, and R. M. Osgood, Jr., "Self-phase-modulation in submicron silicon-on-insulator photonic wires," Opt. Express **14**(12), 5524–5534 (2006).
13. N. K. Hon, R. Soref, and B. Jalali, "The third-order nonlinear optical coefficients of Si, Ge, and $Si_{1-x}Ge_x$ in the midwave and longwave infrared," J. Appl. Phys. **110**(1), 011301 (2011).
14. M. A. Ettabib, K. Hammani, F. Parmigiani, L. Jones, A. Kapsalis, A. Bogris, D. Syvridis, M. Brun, P. Labeye, S. Nicoletti and P. Petropoulos, "FWM-based wavelength conversion in a silicon germanium waveguide," in proceedings of OFC, 17–23 March 2013, Anaheim, OTh1C.4 (2013).
15. K. Hammani, M. A. Ettabib, A. Bogris, A. Kapsalis, D. Syvridis, M. Brun, P. Labeye, S. Nicoletti, D. Richardson and P. Petropoulos, "Linear and nonlinear properties of sige waveguides at telecommunication wavelengths," in proceedings of OFC, 17–23 March 2013, Anaheim, JTh2A.34 (2013).

#186044 - $15.00 USD Received 27 Feb 2013; revised 17 Apr 2013; accepted 17 Apr 2013; published 5 Jul 2013

16. Q. Lin, T. J. Johnson, R. Perahia, C. P. Michael, and O. J. Painter, "A proposal for highly tunable optical parametric oscillation in silicon micro-resonators," Opt. Express **16**(14), 10596–10610 (2008).

1. Introduction

Wavelength conversion based on FWM in $\chi^{(3)}$ media is becoming increasingly attractive for applications in dense high speed wavelength division multiplexed (WDM) networks, where transparency to the bit rate and the modulation format are critical requirements [1]. In recent years research has focused on engineering devices, which, apart from exhibiting strong nonlinear characteristics, they also possess tightly controlled chromatic dispersion profiles, so that high conversion efficiencies, high signal gains and broad operation bandwidths can be achieved. At the same time, the attraction of realizing ultra-fast low power highly nonlinear integrated devices has recently made silicon photonics a hot research topic [2–5]. Several demonstrations of nonlinear effects, such as FWM [9, 10], third-harmonic generation [11], self-phase modulation [12] and Raman amplification [6–8] have already been reported in silicon-on-insulator (SOI) waveguides and nanowires. Furthermore, in contrast to pure silicon, silicon germanium (SiGe) alloys are expected to possess a higher nonlinear coefficient [13]. However, the majority of the work on SiGe has so far focused on the material suitability for applications in the mid- and long-infrared window of the electromagnetic spectrum and there have been very few, if any, studies of the material applicability for signal processing at telecommunications wavelengths.

In this paper, we demonstrate FWM-based wavelength conversion of 40 Gbaud DPSK and QPSK signals at 1.55 μm wavelength using a 2.5 cm long silicon germanium waveguide ($Si_{0.8}Ge_{0.2}$), the first results of which were reported in [14]. An idler with an optical signal to noise ratio (OSNR) of 23 dB was generated with an approximately 2 dB BER conversion penalty both for the cases of DPSK and QPSK signals.

2. Device description

The $Si_{0.8}Ge_{0.2}$ waveguide used in this work was a strip waveguide embedded in Si. The waveguide had a width of 1 μm with a 2 μm taper at the entrance. The length of the taper was 0.5 mm and the total device length was 2.5 cm. The fabrication method consisted of realizing a 1.4 μm thick SiGe layer directly on 200 mm Si substrates. The layer was epitaxially grown by reduced pressure chemical vapor deposition (RP-CVD) to control precisely the Ge percentage and uniformity. The strip was etched using inductively coupled plasma reactive ion etching (ICP RIE) technique and encapsulated by a 12 μm Si cladding layer with the same RP CVD technique. Figure 1 shows a typical scanning electron microscope (SEM) image of the waveguide cross-section before and after encapsulation.

The propagation loss of the waveguide was measured to be 1.4 dB/cm using a Fabry Perot resonance measurement technique, and the two-photon absorption (TPA) coefficient was also measured to be 1.25 cm/GW at 1550 nm. The effective nonlinearity of the waveguide was 25.8 /W/m, as characterized by measuring the nonlinear phase shift of a dual-frequency beat signal [15].

#186044 - $15.00 USD Received 27 Feb 2013; revised 17 Apr 2013; accepted 17 Apr 2013; published 5 Jul 2013

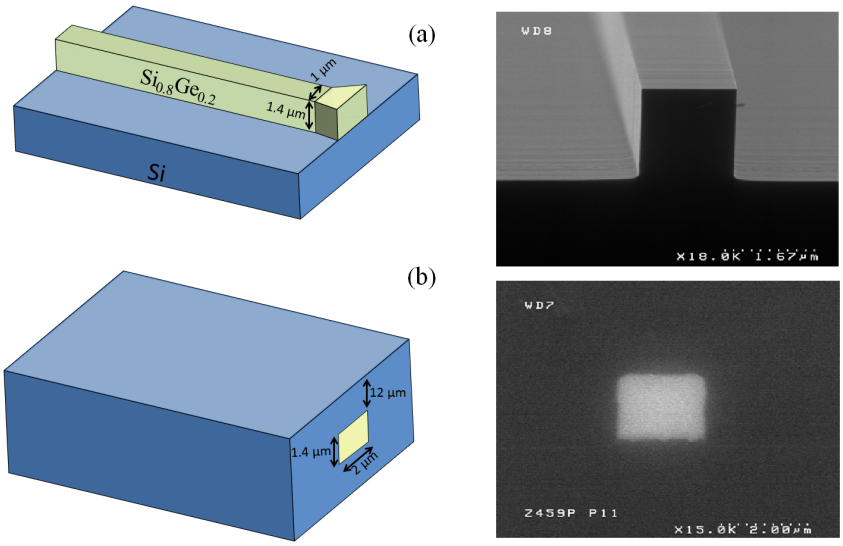

Fig. 1. 1μm wide SiGe strip waveguide before (a) and after (b) encapsulation in a 12μm Si cladding layer. The total device length of 2.5 cm includes a 0.5 mm taper at its entrance.

Alongside the experimental characterization of the waveguide, a numerical model was also developed. The model involves the propagation of pump, signal and idler signals which obeys the following equations [16]:

$$\frac{\partial A_P}{\partial z} = \left\{ i\left(\beta_p + \beta_p^f\right) - \alpha_p / 2 \right\} A_P + i\left(\gamma_p P_p + 2\gamma_{ps} P_s + 2\gamma_{pi} P_i\right) A_P + 2i\,\gamma_{pspi} A_s A_i A_p^* \tag{1}$$

$$\frac{\partial A_s}{\partial z} = \left\{ i\left(\beta_s + \beta_s^f\right) - \frac{\alpha_s}{2} \right\} A_s + i\left(\gamma_s P_s + 2\gamma_{sp} P_p + 2\gamma_{si} P_i\right) A_s + i\,\gamma_{spip} A_i^* A_p^2 \tag{2}$$

$$\frac{\partial A_i}{\partial z} = \left\{ i\left(\beta_i + \beta_i^f\right) - \alpha_i / 2 \right\} A_i + i\left(\gamma_i P_i + 2\gamma_{ip} P_p + 2\gamma_{is} P_s\right) A_i + i\,\gamma_{ipsp} A_s^* A_p^2 \tag{3}$$

where A_j, α_j, β_j are the field, the linear loss and propagation constants with j = {p,s,i} denoting the pump, signal and idler waves respectively. The nonlinear parameter γ_{ijkl} can be calculated provided that Kerr coefficient n_2, two photon absorption β_{TPA}, effective mode area, modal refractive index and mode overlap factors are known for all possible combinations appearing in Eqs. (1)-(3) [16]. The parameters n_2 and β_{TPA} characterize the material. According to [13], Garcia's model, fitted to available experimental measurements, can be utilized to predict the n_2, β_{TPA} evolution of Si, Ge and $Si_{1-x}Ge_x$ alloys for all the wavelengths of interest. Some of the aforementioned quantities must be calculated for the given structure through a waveguiding analysis. By means of a Finite Elements Method (FEM) solver, the effective refractive index, the effective mode area and the modal overlaps can be calculated. In Fig. 2 the field profiles of the fundamental TE and TM modes at 1550 μm are depicted in Fig. 2.

From the waveguide analysis it was concluded that the waveguide is predominantly quasi-TM for the aforementioned width, which can be also observed by noticing that the effective

#186044 - $15.00 USD Received 27 Feb 2013; revised 17 Apr 2013; accepted 17 Apr 2013; published 5 Jul 2013

mode areas for the two polarization states are 1.82308 μm^2 for TM and 1.8508 for TE μm^2 respectively.

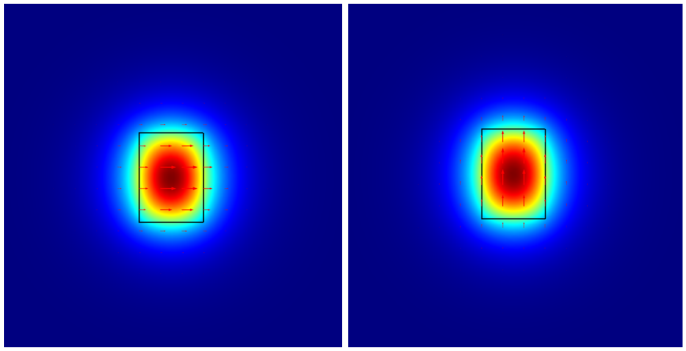

Fig. 2. Field profiles of the TE (left, neff = 3.5238) and TM (right, neff = 3.52422) fundamental modes for waveguide width 1µm height 1.4µm

The linear losses were considered to be around 1.4 dB/cm relying on the experimental findings. The parameter β_j^f represents the free-carrier induced perturbations to the propagation constant described by the Drude model [5]. Finally, the Raman Effect can be safely ignored due to its narrow bandwidth nature in silicon based waveguides [5].

The calculation of the dispersion curve is a very useful tool for the evaluation of the bandwidth of the FWM process in the waveguide. Our analysis showed that within the wavelength band under investigation, dispersion was always normal and quite far from any zero crossing.

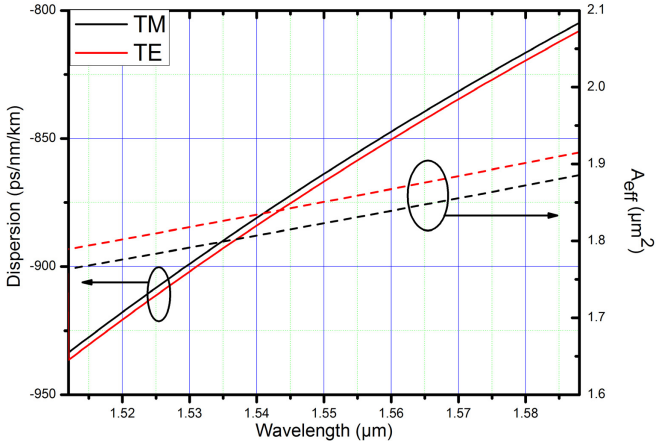

Fig. 3. Dispersion curves for the structure under investigation and effective mode areas as a function of wavelength.

The calculated dispersion curves for the two polarization exes of the waveguide are shown alongside the effective mode area in Fig. 3. As can be seen from the figure, the waveguide was predicted to exhibit −866 ps/nm/km dispersion for TE and −863 ps/nm/km for TM respectively at 1550 nm. Furthermore, based on the numerical simulations of the effective area for the two polarization states, the effective nonlinearity of the waveguide was estimated to be 22.95 and 23.3 /W/km for TE and TM respectively, indicating a close agreement with the experimental measurement reported above.

#186044 - $15.00 USD Received 27 Feb 2013; revised 17 Apr 2013; accepted 17 Apr 2013; published 5 Jul 2013

3. Experimental setup and results

The wavelength converter setup is shown in Fig. 4. Light from a CW pump laser at 1557.36 nm was coupled through an 80/20 coupler with a 40 Gbaud non-return-to-zero DPSK (or QPSK) 2^{31}-1 pseudo-random bit sequence (PRBS) signal. The two signals were then amplified in an erbium doped fiber amplifier (EDFA) and their state of polarization was aligned to the TE polarization axis of the $Si_{0.8}Ge_{0.2}$ waveguide through a polarization controller (PC). A commercial lensed fiber with a spot size of 2 μm was used to launch the signals into the waveguide, and a coupling loss of approximately 4.2 dB was measured, resulting in successfully coupling a total of 290 mW of pump power and 115 mW of signal power into the waveguide, which is well below the experimentally measured TPA threshold of 2.5 W.

At the output, the performance of the wavelength converter was assessed in terms of eye and constellation diagrams, as well as BER measurements. For this purpose, the converted signal (idler) was filtered using a 2-nm tunable bandpass filter and detected. For the BER measurements, the DPSK signal was demodulated using a 1-bit delay line interferometer (DLI) which was followed by an optically pre-amplified receiver, whereas for the QPSK signal, an optically pre-amplified coherent receiver and a real-time data acquisition system were used.

An optical spectral trace obtained at the output of the waveguide for a DPSK input signal with a 3 nm separation from the pump is shown at the bottom left of Fig. 4. The figure shows a FWM conversion efficiency (CE) of ~-18 dB (defined as the ratio of the power of the converted idler to the output signal power). The OSNR of the converted signal was ~23 dB (Res = 0.1nm). The FWM CE as a function of wavelength detuning between the pump and the data signal is also plotted (Fig. 4 (bottom, right)). A 3 dB bandwidth of approximately 22 nm was measured. The figure also compares the measurement with the results obtained from the numerical model, confirming good agreement between the two.

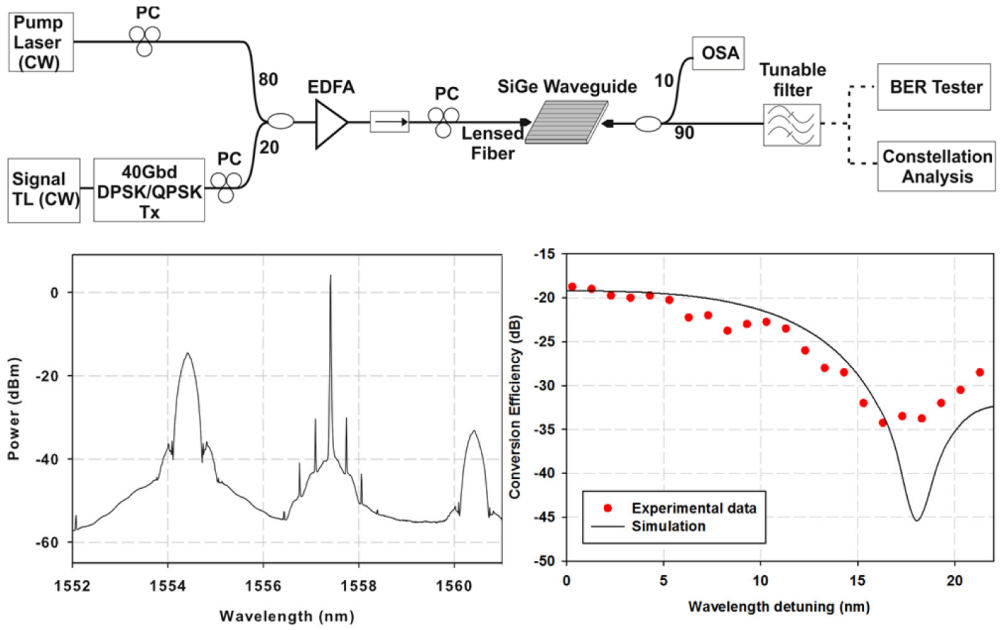

Fig. 4. Top: Experimental set-up used to characterize the wavelength converter. Bottom: spectral trace of FWM measured at the output of the waveguide (left); and numerical calculation (line) and experimental measurement (circles) of FWM conversion efficiency versus wavelength detuning (right).

#186044 - $15.00 USD Received 27 Feb 2013; revised 17 Apr 2013; accepted 17 Apr 2013; published 5 Jul 2013

The FWM CE dependence on the state of polarization was studied next. The use of a polarization controller and a polarizer allowed the angle of polarization of the two co-polarized incident beams to be swept from 0 to 180 degrees and the CE was subsequently measured. The polar plot displayed in Fig. 5 shows a maximum of 1 dB variation in CE as the polarization angle was swept from 0 to 180 degrees.

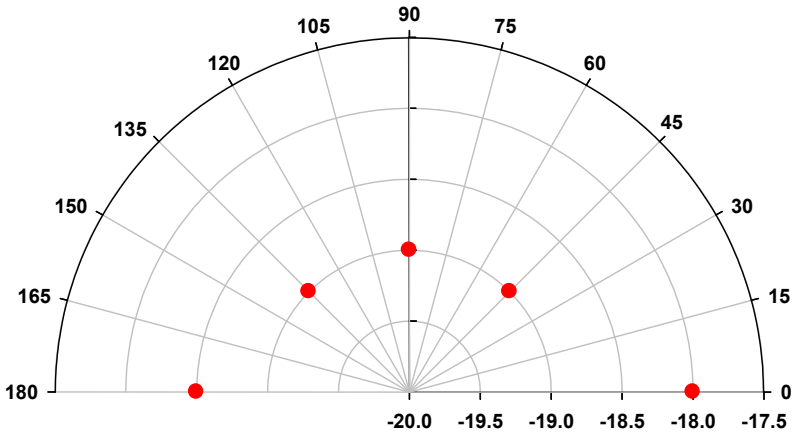

Fig. 5. Polar plot of the conversion efficiency dependence on the angle of polarization.

Figure 6(a) shows constellation diagrams of the original DPSK data signal (B2B) and the converted idler. The B2B measurement exhibited a root-mean-square (rms) error vector magnitude (EVM) of 6.2%, in contrast to the idler for which an rms EVM of 15.27% was measured. Furthermore, the eye diagrams shown in the inset of Fig. 6 (b) show an open eye for the idler, albeit with some degradation in comparison to the B2B. BER measurements revealed an approximately 2.3 dB conversion penalty at a BER of 10^{-9} relative to the B2B.

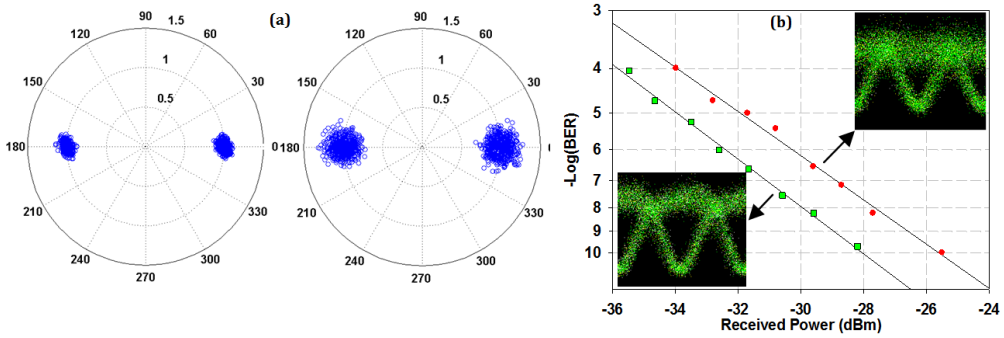

Fig. 6. (a) Constellation diagrams for the original 40 Gbit/s DPSK signal (left) and idler (right)
(b) BER curves and eye diagrams for the B2B (square) and the idler (circle).

Figure 7(a) shows the 40 Gbaud QPSK constellation diagrams for the B2B signal and the converted idler. An rms EVM of 9.7% was obtained for the B2B in contrast to 12.9% for the idler. Furthermore, the BER curves shown in Fig. 7(b) show a 2 dB power penalty at BER = 10^{-3} as a result of the conversion (note that no BER measurements lower than 10^{-6} were possible using the real-time acquisition system).

#186044 - $15.00 USD Received 27 Feb 2013; revised 17 Apr 2013; accepted 17 Apr 2013; published 5 Jul 2013

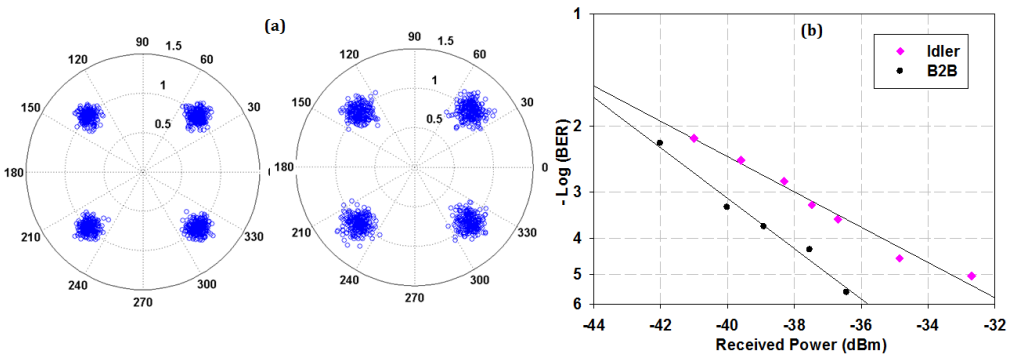

Fig. 7. (a) Constellation diagrams for the 80 Gbit/s QPSK B2B signal (left) and idler (right) (b) BER curves for the B2B signal (circle) and the idler (diamond).

3. Conclusion

We have demonstrated FWM-based wavelength conversion of 40 Gbaud phase shift keyed (PSK) signals in a SiGe waveguide at telecommunication wavelengths. Results show a 2dB power penalty is achievable when pumping the waveguide with power levels well below the TPA threshold. We believe that filtering the EDFA-amplified pump and data signals prior to launching into the waveguide would improve the overall performance of the converter and reduce the conversion penalty even further. Furthermore, significant benefits in the FWM conversion efficiency can be obtained by using a longer device. Theoretical calculations show that by simply doubling the length of the waveguide to 5 cm, the FWM conversion efficiency would be improved by approximately 3.2 dB. Furthermore, significant design insights have been gained through this study and we believe that through adopting a more complex waveguide design and/or germanium concentration profile, both the waveguide nonlinearity and dispersion properties at 1550 nm can be significantly improved, thus making this waveguide technology a potential competitor to other state-of-art nonlinear waveguides.

Acknowledgments

This work was partially supported by the European Communities Seventh Frame-work Programme FP7/2007-2013 under Grant 288304 (STREP CLARITY). Dr. F. Parmigiani gratefully acknowledges the support from the Royal Academy of Engineering/EPSRC through a University Research Fellowship.